This is an Authors' Accepted Manuscript version of the paper:
J. Wurts, J. L. Stein, and T. Ersal, "Collision Imminent Steering Using Nonlinear Model Predictive Control," American Control Conference, Milwaukee, Wisconsin, 2018.

Collision Imminent Steering Using Nonlinear Model Predictive Control

John Wurts, Jeffrey L. Stein, and Tulga Ersal*

Abstract— **Collision imminent steering is an automotive active safety feature designed to swerve and avoid an obstacle on the road if the vehicle detects a forward collision cannot be avoided by braking alone. A collision imminent steering system is formulated in this paper to generate an optimal control sequence that performs an aggressive lane change maneuver in the shortest distance possible in a highway driving environment. The algorithm uses nonlinear model predictive control that pushes the vehicle to its dynamic handling limits, which are established through limits on the tire slip angle. Additionally, the algorithm is developed to leverage active four wheel steering to improve the performance over traditional front only steering. Numerical results show a window exists for which the vehicle can change lanes safely, even at highway speed. A Pareto front is generated to quantify the trade-off between maximum allowable tire slip and safe steering distance.**

I. Introduction

Next generation vehicles are able to exploit an increased amount of sensor information and embedded computing capabilities, which support more sophisticated active safety features. One such emerging feature is collision imminent steering (CIS). In CIS, the vehicle detects when a forward collision cannot be avoided by braking alone and implements a steering command to make, if feasible, a lane change maneuver avoiding the obstacle. The effectiveness of a CIS system thus relies on the minimum distance required to safely change lanes, which pushes the vehicle to its dynamic, and often, nonlinear limits.

In CIS, the optimal steering control sequence or a desired reference trajectory is not necessarily known *a priori*. Hence, the two main technical challenges to be addressed are the construction of an optimization problem that guarantees a collision-free stable solution, and solving said problem for a set of future control inputs, and corresponding state trajectory, that properly accounts for vehicle nonlinear dynamics. To address these challenges, this paper presents an algorithm that solves for a future steering sequence where the corresponding predicted vehicle trajectory reflects the vehicle dynamics and optimizes a set of hard constraints based on a highway environment. This is accomplished using nonlinear model predictive control (MPC).

Early implementations of CIS, also referred to as collision avoidance, use variations of reference trajectory controllers. Often, a reference trajectory is generated first as a straight line between two points on a topographic grid, presenting a start point and a desired trajectory to the end point. Then, obstacle avoidance is introduced as a quadratic state penalty function that a linear controller can minimize online [1]. Alternatively, a reference trajectory can be generated *a priori* as a minimum of a potential function where the distance to an obstacle relates to the potential energy. Then a low level PID controller can navigate the desired course [2]. A key characteristic of this category of methods is that they cannot distinguish between a difficult trajectory and an infeasible trajectory that crashes into an obstacle. Additionally, they must use conservative trajectories to ensure the PID controller is capable of following the reference trajectory.

To ensure a controller can follow a reference trajectory at the dynamic limits of the vehicle, advanced controllers have been developed. One such approach uses an offline optimal trajectory planner to generate the theoretical fastest trajectory through a race course. With a known reference trajectory, an advanced steering controller, properly accounting for vehicle nonlinearity, was able to navigate a passenger vehicle through a race course. While this method can push the vehicle towards its dynamic limits, the desired reference course is still required to be generated *a priori*. Further, tracking a trajectory that is optimized offline does not always exploit the full capability of the vehicle [3].

Recent work has made progress towards overcoming these limitations. Specifically, MPC formulations have been created to generate a control trajectory through an unstructured environment for the purpose of maximizing the mobility of a vehicle even during obstacle avoidance without *a priori* information [4], [5]. However, these formulations are not designed as an active safety feature to wait until the last possible instance to intervene, a requirement of CIS.

Researchers also studied methodologies to alleviate the impact of a collision if it cannot be avoided. One such example demonstrates a vehicle initiating a spin to mitigate a T-bone collision by causing a side-side collision [6]. In this scenario, the initial state is known, and the final vehicle rotation defined, but the control sequence and progression of remaining states are not known . In this case, MPC was used to rotate the vehicle 90° in the minimum amount of time, but did not incorporate specific environmental constraints relevant to a lane change.

In the context of a lane change maneuver, a linearized vehicle model was previously used to investigate blended control for near-collision encounters in [7]. In this work two lanes were modeled and an MPC controller was used to change lanes. However, the host vehicle was traveling significantly slower than highway speeds and the controller was designed to avoid the vehicle's dynamic limits, as the

* Corresponding author (tersal@umich.edu)
J. Wurts, J.L. Stein, and T. Ersal are with the Department of Mechanical Engineering, University of Michigan, Ann Arbor, MI.

Toyota Research Institute (TRI) provided funds to assist the authors with their research. This article solely reflects the opinions and conclusions of the authors and not TRI or any other Toyota entity.

methodology only addresses linearized system dynamics.

Compared to the state-of-the-art, the CIS system presented in this paper has two novel contributions. First, an objective function and set of constraints are derived from the highway lane environment and vehicle stability analysis in terms of side slip. Second, a nonlinear MPC formulation is developed that discretizes the future states in a manner that ensures the control sequence matches expected states, and the discretization is C^2 smooth for gradient-based optimization. Combined, these two features allow the optimizer to solve simultaneously for a matching control sequence and trajectory for a lane change, and said trajectory is guaranteed to be collision free under the working assumptions.

The remainder of this paper is organized as follows. Sec. II details the highway driving environment, host vehicle, and the criteria for a successful lane change. Sec. III defines the optimization problem and numerical formulation, as well as details specific to the MPC implementation. Sec. IV presents the numerical simulation results for the optimal lane change, and discusses the trade-off of allowable tire slip and performance using a Pareto front. Conclusions and suggested future directions are given in Sec. V.

II. Highway Driving Environment and Vehicle Dynamics Model

A highway driving environment is challenging due to the speeds at which the CIS maneuver must take place and the space available to maneuver. The CIS system is intended to perform an aggressive lane change maneuver when it detects a forward collision is imminent and the vehicle has passed the safe braking threshold. The safe braking threshold can be estimated theoretically by calculating the distance the vehicle would need to come to a full stop at maximum deceleration.

In limit braking, the vehicle slows at its maximum deceleration defined by the coefficient of friction. The results presented in this paper are based on a coefficient of friction of 0.8 and a vehicle speed of 30 m/s. This coefficient of friction represents standard tires on dry pavement [6], and this speed represents 67 mph (108 kph), which is a reasonable highway speed in The United States. Based on these values, a vehicle traveling at 30 m/s decelerating to 0 m/s at $0.8g$ requires a stopping distance of 57.3 m over 3.82 s.

Alternatively, the proposed CIS algorithm calculates a set of future control inputs for which the corresponding trajectory changes lanes in the shortest distance possible. At a high level, the intended trajectory must satisfy three criteria: the vehicle must completely change lanes prior to passing the obstacle, the vehicle cannot exceed the lane boundary of the lane it changes into, and the vehicle must stabilize in the next lane. Fig. 1 illustrates a successful lane change, and mathematical formulation of these three criteria are derived in Sec. III.

The second notable characteristic of the highway environment is the space allotted to the lanes. Based on United States building code, the minimum lane width is set at $y_{\text{lane}} = 3.7$ m, implying a half-width of 1.85 m [8].

The host vehicle is modeled as a 3 degrees of freedom (3DoF) bicycle model with four wheel steering using the nonlinear Pacejka tire model [6]. This decision is based on prior work that has shown that this level of detail is sufficient for MPC-based obstacle avoidance even at the dynamic limits when obstacles are not significantly wide [9]. Further, four wheel steering has previously been shown to improve vehicle tracking of a predefined trajectory [10], and is currently available in many luxury vehicle models. For this paper, the 3DoF vehicle model is used both as the plant model and the MPC model as a first step in the investigation of the proposed concept.

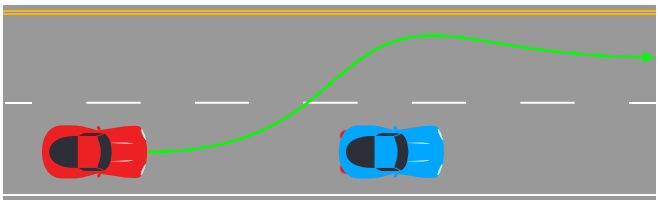

Fig. 1. A topographical view of a successful lane change. The host vehicle starts at the left side of the image and travels to the right. The vehicle's center of gravity trajectory is depicted as a solid green line. The host vehicle clears the starting lane boundary before passing the obstacle, stays within the second lane outer boundary, and has a stable trajectory at the end of the maneuver.

TABLE I

Host vehicle parameters based on 2017 BMW 740*i*. The upper table is values from manufacturer's technical specification. The lower table is values derived as needed for 3DoF model.

Vehicle Parameter	Parameter Symbol	Value
Vehicle mass	m	2041 kg
Weight Distribution	-	51.4/48.6 F/R
Wheel Base	-	3.2 m
Vehicle Width	-	1.8 m
Front wheel to CG distance	l_f	1.56 m
Rear wheel to CG distance	l_r	1.64 m
Yaw moment of inertia	I_{zz}	4964 kg $\cdot$ m^2

The vehicle parameters used in this work are based on a luxury sedan and are reported in Table I. Most of these parameters are readily available from manufacturer's published technical specifications and remaining parameters are estimated for a sedan [11].

Recall that the intention of the system is to change lanes in the shortest distance possible. The 3DoF model only considers the vehicle's CG position; thus the lane change criteria must be adjusted to include the vehicle half width to avoid body clipping. The lane change threshold, $y_{\text{threshold}}$, is set at 3.25 m, corresponding to 1.85 m for lane half width plus 0.9 m for vehicle half width plus 0.50 m as a buffer. Similarly, the outer lane boundary, y_{outer}, is set at 4.15 m, corresponding to 5.55 m for one and a half lane widths minus 0.9 m for vehicle half width minus 0.50 m as a buffer.

As an initial simplification, the CIS system only has control over the steering and is not allowed to modify the vehicle speed. Accordingly, the 3DoF vehicle model is modified to maintain constant longitudinal velocity. Further, all longitudinal forces in the vehicle frame are simplified to zero as they are significantly smaller than the lateral forces.

The states of the vehicle model are detailed in (1), control input in (2), and simplified vehicle dynamics in (3).

$$\mathbf{x} = \begin{bmatrix} \text{global x position [m]} \\ \text{global y position [m]} \\ \text{vehicle yaw [rad]} \\ \text{longitudinal velocity [m/s]} \\ \text{lateral velocity [m/s]} \\ \text{yaw rate [rad/s]} \\ \text{front steering angle [rad]} \\ \text{rear steering angle [rad]} \end{bmatrix} = \begin{bmatrix} x \\ y \\ \psi \\ u \\ v \\ \omega \\ \delta_f \\ \delta_r \end{bmatrix} \tag{1}$$

$$\mathbf{u} = \begin{bmatrix} \text{front steering rate [rad/s]} \\ \text{rear steering rate [rad/s]} \end{bmatrix} = \begin{bmatrix} \dot{\delta}_f \\ \dot{\delta}_r \end{bmatrix} \tag{2}$$

$$\frac{d\mathbf{x}}{dt} = \begin{bmatrix} u\ \cos(\psi) - v\ \sin(\psi) \\ u\ \sin(\psi) + v\ \cos(\psi) \\ \omega \\ 0 \\ -u\ \omega + \frac{F_{y,f}\cos(\delta_f) + F_{y,r}\cos(\delta_r)}{m} \\ \frac{F_{y,f}\cos(\delta_f) l_f - F_{y,r}\cos(\delta_r) l_r}{I_{zz}} \\ \dot{\delta}_f \\ \dot{\delta}_r \end{bmatrix} \tag{3}$$

Here, $F_{y,(f,r)}$ is the tire force in the lateral frames of the front and rear tires, respectively. Additionally, the global coordinate frame is aligned such that the x axis is parallel to the lane, and y axis is perpendicular to the lane.

The tire lateral force is calculated in (4) based on the Pacejka tire formula. The tire parameters and variables are defined in Table II. These tire properties are chosen to represent a tire with maximum grip of $0.8g$, peak lateral force at 12° slip, and 10% force relaxation at high slip. The parameter l is taken as l_f for front wheel velocities and $-l_r$ for rear wheel velocities, in accordance with vehicle yaw rate.

$$\begin{aligned} F_y &= \mu F_z \sigma_y \\ \sigma_y &= -\frac{V_y}{V_x}\sin(C\ \arctan(B\frac{V_y}{V_x})) \\ V_x &= u\ \cos(\delta) + (v + \omega l)\sin(\delta) \\ V_y &= -u\ \sin(\delta) + (v + \omega l)\cos(\delta) \end{aligned} \tag{4}$$

(3) and (4) dictate the nonlinear system dynamics. In the next section, the system dynamics are used to develop an MPC formulation for the CIS maneuver.

III. Optimal Control Problem and Model Predictive Control Formulation

The MPC implementation developed in this work uses a direct shooting method solved using forward Euler integration expressed as follows.

$$\begin{aligned} \mathbf{x}(t_{i+1}) &= \mathbf{x}(t_i) + t_s\ \frac{d\mathbf{x}}{dt}\Big|_{t=t_i} \\ \mathbf{x}(t_0) &= \begin{bmatrix} 0 & 0 & 0 & u_0 & 0 & 0 & 0 & 0 \end{bmatrix}^T \end{aligned} \tag{5}$$

There are two distinct phases of the MPC: propagating the dynamics forward and evaluating the resulting trajectory. The differential equations describing the vehicle dynamics do not have a closed form solution. Therefore, a numerical integration scheme is used, and the MPC is developed to handle the explicit integration points. This formulation incorporates the system dynamics constraints automatically in the forward Euler method; thus they are not explicitly defined in the optimization problem.

Piecewise constant control inputs are used to simulate modern automotive communication networks that use loop timing. The algorithm solves for a series of constant front steering and rear steering rates, where each pair is executed by the vehicle for a time length of t_c. The algorithm uses a prediction horizon of length t_h, which can be a non-integer multiple of t_c. Additionally, the forward Euler method uses an integration time step of t_s, which should be an integer divisor of t_c. For this implementation, an integration time step of $t_s = 10$ ms and a control input length of $t_c = 100$ ms are used, as 10 Hz is a reasonable loop time in automotive applications. Offline analysis showed 10 ms integration steps as fine enough to accurately simulate the dynamics without excessive computational cost. In the absence of a general method for determining the proper time horizon in MPC, numerical testing was performed and $t_h = 2.51$ s was found to work well for this scenario.

The mathematical representation of the objective function and constraints are derived in the following subsections.

TABLE II

Tire Properties

Tire Parameter	Parameter Symbol	Value
Coefficient of Friction	μ	0.8
Tire Property	B	13
Tire Property	C	1.285
Tire Longitudinal Velocity	V_x	
Tire Lateral Velocity	V_y	

A. Objective Function: Distance to Clear Obstacle

The CIS system is designed to minimize the x distance traveled when the vehicle safely crosses into the next lane. This formulation allows a higher level controller to wait as long as possible before overriding the human driver. Numerically, this discrete lane change event occurs at the vehicle's x position when the vehicle's y position exceeds $y_{\text{threshold}}$. The x position when crossing the threshold is found through a linear interpolation between the integration points before and after crossing, represented by $\mathbf{x}_k$ and $\mathbf{x}_{k+1}$, respectively. Thus, the objective function is expressed as follows.

$$x_{\text{obj}}(\mathbf{x}_k, \mathbf{x}_{k+1}) = x_k + \frac{y_{k+1} - y_k}{x_{k+1} - x_k}(y_{\text{threshold}} - y_k) \tag{6}$$

B. Nonlinear Tire Constraint

Often, the lateral force of modern automotive tires relaxes at high slip angles. As a result, local minima occur that can be challenging for gradient based optimization. To avoid local minima when solving the MPC optimization, constraints are implemented on the tire slip angle.

Fig. 2 plots the normalized tire force versus the tire slip angle for pure longitudinal velocity. In this model, the front

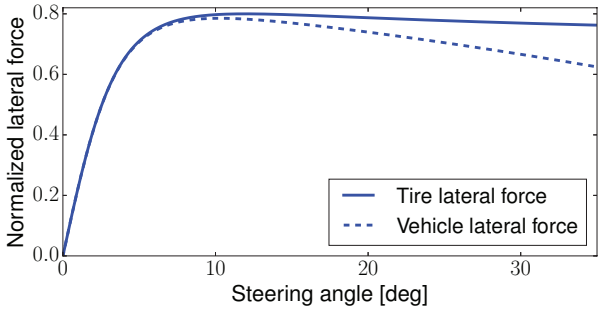

Fig. 2. The lateral force in the tire frame is plotted in solid blue, and the lateral force in the vehicle frame is plotted in dashed blue. Due to the coordinate transformation, at high slip angles the vehicle lateral force decays faster than the tire lateral force.

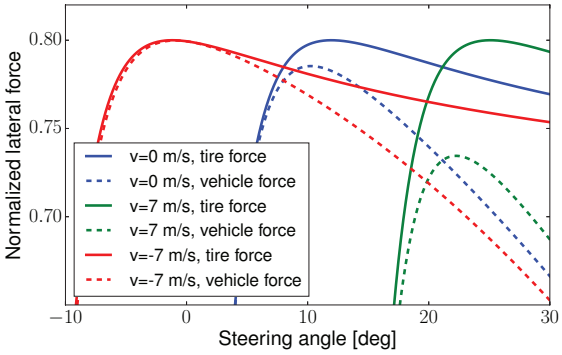

Fig. 3. The same variables of Fig. 2 are plotted, but for variations in vehicle lateral velocity. For this example, vehicle yaw rate is zero.

and rear tires have the same normalized performance, but actual tire force will vary due to differences in weight distribution. For this tire model, only the lateral force is considered; the longitudinal tire force is assumed to be zero.

Additionally, the normalized lateral force in the vehicle frame is plotted, which is the tire lateral force rotated by $\cos(\delta)$. At small angles, the tire lateral force mirrors to the vehicle lateral force, but at high slip angles the vehicle lateral force decays faster than the tire lateral force with increasing slip angle.

Fig. 2 shows there are two local minima of the lateral forces. For $\delta \in [0°, 35°]$, the minimum lateral forces occur at 0° and 35°. As a result, at high slip angles, gradient based optimization would have numerical difficulty. For example, if the tires are at 20° steering angle, then they create a lateral force in positive y, causing a turn. If the optimizer wanted to return the vehicle to straight, the gradient information of the vehicle lateral force would indicate reducing lateral force is achieved by increasing the steering angle. This causes a local minima where the optimizer would not command the steering angle to zero.

Without any countermeasures, entering this local minimum is highly likely because the algorithm is designed to push the vehicle to its dynamic limits. As a result, a new constraint is introduced to avoid local minima in the tire force. In Fig. 2, the steering angle and slip angle are equal, because the vehicle is traveling purely straight ahead. When the vehicle experiences a non-zero lateral velocity and yaw rate, this is not necessarily true; see, e.g., Fig. 3 showing differences in the tire and vehicle forces due to three variations in the lateral velocity. Note the steering angle that produces the peak lateral force shifts as a function of the lateral velocity, and by extension, yaw rate.

The stable tire region is where $\frac{dF_y}{d\delta} > 0$, because this is the region where the gradient information can return the steering wheels to neutral. Fig. 3 shows simply limiting the steering angle does not ensure the optimizer remains in the stable region. By introducing lateral velocity, the tire force and vehicle force plots are translated and slightly stretched. For given lateral velocities and yaw rates, there is a neutral steering angle where the tires do not generate lateral force. The slight stretching effect means limiting the steering angle to $\pm 8°$ of the neutral steering angle does not ensure a stable tire region, either. When the vehicle is traveling straight forward, the difference in steering angle where the peak tire force and peak vehicle force occurs is approximately 4°. However, when lateral velocity is introduced, the steering angle for peak vehicle force changes, and the difference between peak tire and vehicle force angles changes, as well.

Defining the tire stability constraint by $\frac{dF_{\text{vehicle}}}{d\delta} > 0$ ensures the steering angle is stable and that the optimizer can make full use of the peak vehicle lateral force. However, numerical simulation of the lane change maneuver shows only moderate lateral velocity and yaw rate. Separate analysis of various combinations of lateral velocity and yaw rate shows that limiting the slip angle to $\alpha_{\text{peak}} = 8°$ maintains stability. While this does not allow the optimizer to make maximum use of the available tire force, there are diminishing returns near the peak slip angle. 8° allows for the use of 98% of peak tire force, improves computational cost, and suits the Pareto front analysis in Sec. IV.

The slip angle is defined in (7), and corresponding slip angle constraint in (8).

$$\alpha = \delta - \arctan\left(\frac{v + \omega l}{u}\right) \tag{7}$$

$$\alpha(t_i) \leq \alpha_{\text{peak}} \;\forall\; t \in [t_0, t_h] \tag{8}$$

The slip angle constraint on the front and rear tires is enforced at every integration point in the state trajectory. Depending on the number of integration points used, there can be a significantly large number of constraints, which increases the computational complexity. Alternatively, a switching quadratic function is introduced as a constraint aggregation method. In general, a set of constraints enforced at each integration point is represented as a single constraint shown in (9).

$$g(\xi,\ \xi_{\text{peak}}) = \sum_{i=1}^{n} H(\xi_i - \xi_{\text{peak}})\ (\xi_i - \xi_{\text{peak}})^2 \tag{9}$$

(9) uses the Heaviside step function, $H(x)$, which is zero for arguments below zero and one for arguments above zero. This switching aspect allows the constraint to be a quadratic with respect to the set of ξ that violate the ξ_{peak} parameter. Additionally, this constraint aggregation is C^2 smooth, which is well suited for gradient based optimization. (9) is non-negative and equal to zero when all ξ states are below ξ_{peak}.

As a result, this constraint is posed as an equality constraint for numerical optimizer efficiency.

C. Lane Constraint

Previously in Sec. II, the outer lane criterion was described and a numerical value for the outer threshold derived from the lane and vehicle widths. Based on the global coordinate frame's alignment with the lanes, the outer lane boundary constraint is enforced purely based on the vehicle's y position. The lane constraint is represented in (10). Using the same constraint aggregation as the slip angle, the lane boundary constraint is implemented following (9).

$$y(t_i) \leq y_{\text{outer}} \;\forall\; t_i \in (t_0, t_h] \tag{10}$$

D. Stable Terminal State

In the context of highway driving environment, it is important for the final trajectory to return to a stable trajectory in the next lane. A candidate trajectory is considered stable in this work if the vehicle is traveling purely straight ahead in the next lane at the end of the prediction horizon. Specifically, a stable trajectory is defined by (11).

$$\mathbf{x}_{\text{stable}} = \begin{bmatrix} x & y_{\text{lane}} & 0 & u_0 & 0 & 0 & 0 & 0 \end{bmatrix}^T \tag{11}$$

The stable state is defined recursively with regards to the terminal x position. This implies the optimizer does not seek to adjust the final x position, which is consistent with the evasive maneuver; the optimizer only looks to reduce the x position when crossing the obstacle, not the terminal x position. Matching the enforced seven states at the final integration step are introduced as seven equality constraints.

E. Steering Rate and Steering Angles

The final constraint set is to address the physical limitations of the vehicle. Specifically, the front and rear wheels are both steering angle and rate limited. Typical front wheels have a steering angle range of $\pm 35°$, i.e., $\delta_{\text{front,max}} = 35°$. As an approximate benchmark for the rate limit, a human driver is estimated to traverse three complete rotations of the steering wheel, spanning full left to full right, in approximately 1.0 s. The corresponding 70° of tire steering gives an approximate allowable steering rate of $\dot{\delta}_{\text{front,max}} = 1.2$ rad/s.

Rear wheels in active rear steering vehicles are not consciously controlled by the driver, but rather by an on-board controller that manages a drive-by-wire system. Active rear steering equipped vehicles have smaller ranges of motion on the rear wheels, approximately $\delta_{\text{rear,max}} = 10°$, and lower steering rates, approximately $\dot{\delta}_{\text{rear,max}} = 0.6$ rad/s.

This CIS formulation can handle conventional steering architectures by setting the rear steering rate at 0 rad/s.

F. Optimization Problem

The optimization problem is posed in (12) by incorporating the previously defined objective function and various constraints. The constraint on steering rate does not use the same constraint aggregation in (9), because the steering rate is a linear constraint with respect to the design variables and thus implemented as bounds in numerical optimization.

$$\begin{aligned}
\min_{\mathbf{u}} \quad & x_{obj}(\mathbf{x}_k, \mathbf{x}_{k+1}) & \\
\text{subject to} \quad & g(\mathbf{y},\ y_{\text{outer}}) & = 0 \\
& g(\alpha_{\text{front}},\ \alpha_{\text{peak}}) & = 0 \\
& g(\alpha_{\text{rear}},\ \alpha_{\text{peak}}) & = 0 \\
& g(\delta_{\text{front}},\ \delta_{\text{front,max}}) & = 0 \\
& g(\delta_{\text{rear}},\ \delta_{\text{rear,max}}) & = 0 \\
& \mathbf{x}(t_h)_i - (\mathbf{x}_{\text{stable}})_i & = 0 \;\forall\; i \in [2,8] \\
& |\dot{\delta}_f(t_i)| & \leq \dot{\delta}_{\text{front,max}} \\
& |\dot{\delta}_r(t_i)| & \leq \dot{\delta}_{\text{rear,max}}
\end{aligned} \tag{12}$$

IV. Numerical Results

(12) is transcribed into Python for a proof-of-concept numerical simulation. Based on the limits for peak slip angle shown in Sec. III-B, α_{peak} is set at 8°. An open source implementation of SLSQP is used to solve the nonlinear optimization problem, and solves in approximately 7 minutes on a Chromebook hardware platform using a Intel Celeron 1.60 GHz processor.

Fig. 4 shows four concurrent plots as the vehicle carries out the optimal trajectory. The top pane shows the x-y trajectory of the CG. The solid orange block represents the obstacle that fully blocks the lane and is located just as the optimal trajectory has completely left the original lane. The star on the CG trajectory at the crossing of the obstacle denotes the crossing of $y_{\text{threshold}}$. After clearing the obstacle, the center line of the next lane is plotted in a green dashed line to show the desired stable trajectory at the end of the maneuver. Additionally, the outer lane threshold is shown with a red dashed line with the x-y trajectory coming close

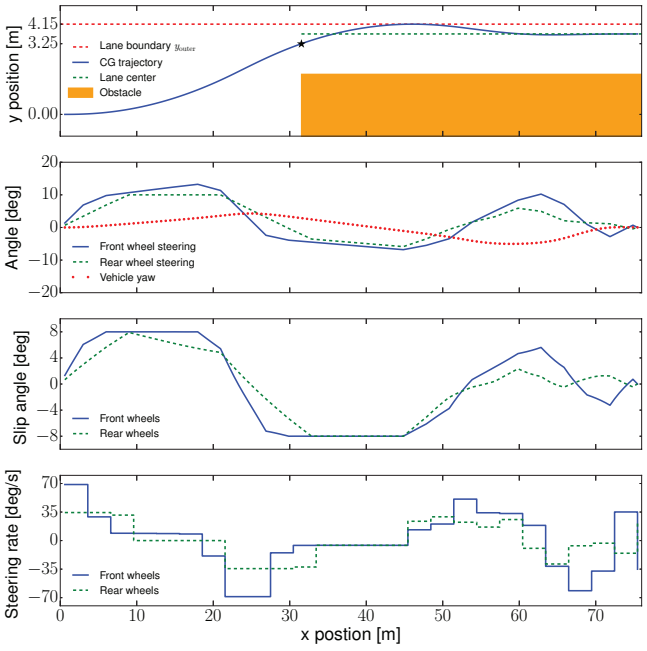

Fig. 4. The four concurrent plots, plotted against x position of the maneuver, show the various states and control inputs during the aggressive lane change.

to the limit. The second plot shows the steering angle of the front and rear tires, as well as vehicle yaw angle, plotted against the x position of the trajectory. The vehicle makes an aggressive turn to the left to initiate the maneuver, but then varies the steering angle to maintain the front and rear slip angles at their limits. The third plot shows the instantaneous slip angle on the front and rear tires. The algorithm attempts to push the tires to the peak lateral force as quickly as possible in the trajectory, then turns back to avoid exceeding the lane boundary. The fourth plot details the control input for each time interval t_c. The rear wheel steering command reaches both the steering angle and steering rate constraint, implying the assumed mechanical performance of the rear steering mechanism is a limiting factor. It is feasible that the system performance could be improved by improving the capabilities of the rear steering system.

For the vehicle model described, the optimal lane change requires 31.0 m to safely change lanes, 46% less than the 57.3 m required by limit braking. By this result, there is 26.3 m of travel after which the vehicle cannot brake in time, but can swerve safely to avoid the collision.

An important result of the optimal solution versus an expected response from a human driver is when the vehicle initiates the first turn to the right. In the case of the optimal solution, the vehicle begins to turn to the right prior to clearing the obstacle. This is arguably counter-intuitive to the average human driver, as a panic reaction is likely to be to hold the left turn until the obstacle is cleared. The optimizer does not hold the left turn, because then the later state trajectory would push beyond the lane boundary. The optimizer is likely able to outperform a common driver, and certainly a distracted driver, because the optimizer appropriately balances current and future actions with later state trajectory predictions.

The slip angle can be a crude measure of the aggressiveness of the maneuver, because higher slip angles generate higher lateral forces. This implies a direct trade-off in maximum allowable slip angle versus distance to clear, as lower slip angles cannot initiate the turn as aggressively. By varying the maximum allowable slip angle and reevaluating (12), a Pareto front is generated in Fig. 5.

The effect of diminishing returns in increasing the maximum allowable slip angle is evident in the Pareto front. At higher slip angles, there is only a slight improvement in performance. However, even at small allowable slip angles, the distance to clear the obstacle outperforms limit braking.

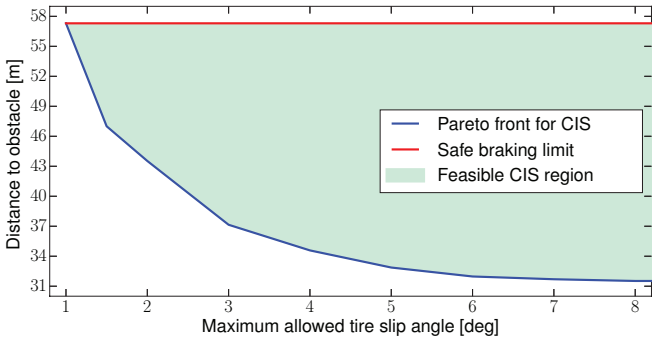

Fig. 5. Increasing the maximum allowable slip angle improves the effectiveness of the CIS system, but with diminishing returns.

V. Conclusion

In this work, a CIS algorithm is formulated as a nonlinear control problem to change highway lanes in the shortest distance possible. This work incorporates specific constraints on the environment to ensure an optimal solution is collision free and avoids crossing the outer lane boundary. Additionally, constraints addressing nonlinearity of the tire forces are developed to avoid local minima during the optimization.

The resulting optimal trajectory changes lanes in a distance significantly shorter than limit braking, showing that a window exists where the vehicle cannot simply brake to avoid collision, but can swerve to safely change lanes. Additionally, it is shown there are diminishing returns of the effectiveness of the algorithm when pushing to the vehicle handling limits.

Future work is focused on expanding the context to curved roads, investigating alternative problem formulations such as minimizing the peak slip angle in the predicted trajectory, and improving the computational speed.

Acknowledgments

The authors thank Alex Cunningham from TRI for his feedback in formulating the collision imminent steering algorithm in accordance with modern automotive architectures.

References

[1] J.-M. Park, D.-W. Kim, Y.-S. Yoon, H. J. Kim, and K.-S. Yi, "Obstacle avoidance of autonomous vehicles based on model predictive control," *Proceedings of the Institution of Mechanical Engineers, Part D: Journal of Automobile Engineering*, vol. 223, no. 12, pp. 1499–1516, 2009.

[2] M. A. Abbas, R. Milman, and J. M. Eklund, "Obstacle avoidance in real time with nonlinear model predictive control of autonomous vehicles," *Canadian Journal of Electrical and Computer Engineering*, vol. 40, no. 1, pp. 12–22, 2017.

[3] V. A. Laurense, J. Y. Goh, and J. C. Gerdes, "Path-tracking for autonomous vehicles at the limit of friction," in *American Control Conference (ACC), 2017*. IEEE, 2017, pp. 5586–5591.

[4] J. Liu, P. Jayakumar, J. L. Stein, and T. Ersal, "Combined speed and steering control in high speed autonomous ground vehicles for obstacle avoidance using model predictive control," *IEEE Transactions on Vehicular Technology*, vol. 66, no. 10, pp. 8746–8763, 2017.

[5] ——, "A nonlinear model predictive control formulation for obstacle avoidance in high-speed autonomous ground vehicles in unstructured environments," *Vehicle System Dynamics*, pp. 1–30, 2017.

[6] I. Chakraborty, P. Tsiotras, and R. S. Diaz, "Time-optimal vehicle posture control to mitigate unavoidable collisions using conventional control inputs," in *American Control Conference*, 2013, pp. 2165–2170.

[7] S. J. Anderson, S. C. Peters, T. E. Pilutti, and K. Iagnemma, "An optimal-control-based framework for trajectory planning, threat assessment, and semi-autonomous control of passenger vehicles in hazard avoidance scenarios," *International Journal of Vehicle Autonomous Systems*, vol. 8, no. 2-4, pp. 190–216, 2010.

[8] A. A. O. S. Highway and T. Off, *A Policy on Geometric Design of Highways and Streets 2001*. American Association of State Highway Transport., 2001.

[9] J. Liu, P. Jayakumar, J. L. Stein, and T. Ersal, "A study on model fidelity for model predictive control-based obstacle avoidance in high-speed autonomous ground vehicles," *Vehicle System Dynamics*, vol. 54, no. 11, pp. 1629–1650, 2016.

[10] A. Alleyne, "A comparison of alternative obstacle avoidance strategies for vehicle control," *Vehicle System Dynamics*, vol. 27, no. 5-6, pp. 371–392, 1997.

[11] G. J. Heydinger, R. A. Bixel, W. R. Garrott, M. Pyne, J. G. Howe, and D. A. Guenther, "Measured vehicle inertial parameters-NHTSAs data through November 1998," SAE Technical Paper, Tech. Rep., 1999.